An Antarctica-to-Spain HF ionospheric radio link: Sounding results

C. Vilella,[1] D. Miralles,[1] and J. L. Pijoan[1]

Received 12 December 2007; revised 28 March 2008; accepted 10 April 2008; published 13 August 2008.

[1] Our research group in Electromagnetism and Communications is involved in a project dealing with the channel characterization of an ionospheric radio link from the Spanish Antarctic Base (62.6°S, 60.4°W) to the Observatori de l'Ebre (40.8°N, 0.5°E) in Spain. Since the link was established for the first time on December 2003, the sounder and measurement techniques have been improved on the basis of the preliminary results. In this paper, the final results of the project corresponding to the 2006/2007 sounding survey are presented. First the hardware and measurement techniques used to probe the channel are described. Then the results in terms of channel availability (and its daily, hourly, and frequency variation), multipath and Doppler spreads, and signal-to-noise ratio are discussed. These results are being used to design the physical layer of a low data rate transmission system intended to send the information acquired by a geomagnetic sensor in the Antarctica.

Citation: Vilella, C., D. Miralles, and J. L. Pijoan (2008), An Antarctica-to-Spain HF ionospheric radio link: Sounding results, *Radio Sci.*, *43*, RS4008, doi:10.1029/2007RS003812.

1. Introduction

[2] From its earliest stages, the development of radio science has been a paradigmatic case of a good understanding between both technology and science. Moreover, they help each other; there exists a mutual feedback in their steps forward. Knowledge acquired on the characteristics of the channel does not only improve the performance of high frequency communication systems but also develops ionospheric science.

[3] The oblique sounding technique is frequently used to obtain the characteristics of the ionospheric channel for a given link. In the literature, many papers related to oblique sounding surveys exist. Most of them concentrate on a specific latitude where single-hop links are preferred in order to describe the propagation conditions (e.g. *Wagner et al.* [1995] and *Angling et al.* [1998] for the high latitudes, *Gibson et al.* [1995] and *Warrington and Stocker* [2003] for midlatitudes, *Fitzgerald et al.* [1999] and *Rao et al.* [2002] for low latitudes). These studies frequently involve a number of measurements, such as amplitude, signal-to-noise ratio (SNR), fading and delay and Doppler spread. However, similar analysis for very long distance links covering simultaneously different latitudes in both hemispheres are rarely found. Although the results obtained from the measurements of such links would be complex to interpret in terms of ionospheric physics, they may give valuable information of the overall ionospheric propagation. For this purpose, we have carried out a new project called SANDICOM (Sounding System for Antarctic Digital Communications) intended for studying the ionospheric link from the Antarctica to Spain. In order to establish this beyond line of sight radiolink some important aspects that determine the feasibility of the communication have been taken into consideration: the attenuation, the Doppler spread, the multipath spread, the SNR and the interference. On the basis of this information SANDICOM has been improved during the last four years. Nowadays, SANDICOM is a sounding system between the Antarctic Spanish Base in Livingston Island (62.6°S, 60.4°W) and the Observatori de l'Ebre in Spain (40.8°N, 0.5°E). The ground range of this path is approximately 12,700 km, so the minimum number of ionospheric reflections (hops) is four.

[4] In addition to the scientific interest of this sounding, a further objective of the project is the establishment of a backup link for data transmission from the remote sensors in the Antarctica. In this context, the ionospheric communications seem to be an interesting complementary alternative to geostationary satellite communications since the latter are expensive and not always available from high-latitudes. Thus the channel measurements are

[1]Grup de Recerca en Electromagnetisme i Comunicacions (GRECO), Enginyeria i Arquitectura La Salle (Universitat Ramon Llull), Barcelona, Spain.

0048-6604/08/2007RS003812

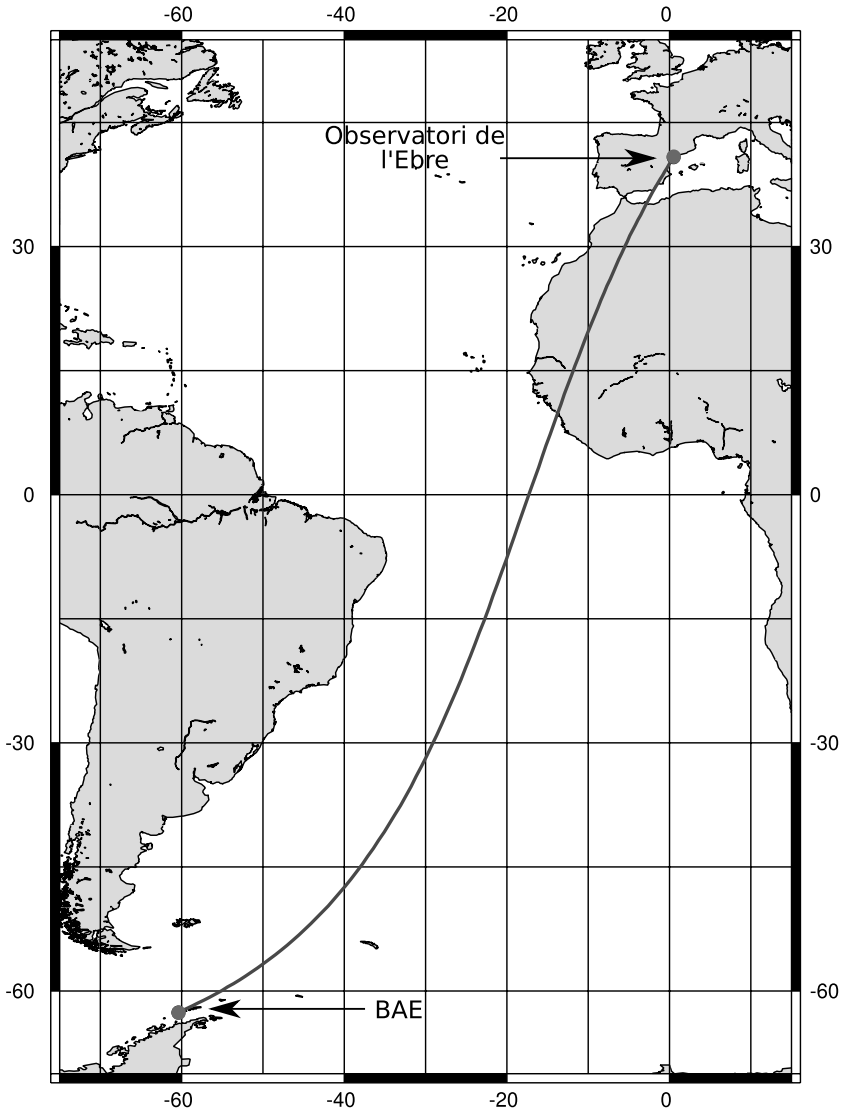

Figure 1. Geographical link characteristics. The transmitter is located in Livingston Island (62.6°S, 60.4°W) and the receiver is placed in the Observatori de l'Ebre (40.8°N, 0.5°E).

being used to design and implement the physical layer of a new radiomodem.

[5] SANDICOM operated for the first time in December 2003. The feasibility of the radiolink was shown during the 2003/2004 sounding campaign [*Vilella et al.*, 2005a]. That year the sounding system was based on standard HF transceivers with a 3-KHz channel bandwidth. It allowed us to perform a preliminary analysis of the channel availability and multipath and Doppler spread measurements.

[6] During the 2004/2005 survey, the transmitter was brought up-to-date with a new digital platform using field programmable gate arrays (FPGA), application specific integrated circuits (ASIC) and a high speed D/A converter. The only analog components of the transmitter were the power amplifier and the antenna coupler. Although this system permitted the generation of an HF signal with any bandwidth, a maximum of 6 KHz was used due to restrictions in the receiver architecture. The results from this sounding campaign are described by *Vilella et al.* [2005b].

[7] During the 2005/2006 survey the receiver was replaced with a new FPGA-based platform [*Vilella et al.*, 2006b], where only some filtering and amplification

Table 1. Emitter, Receiver, and an Estimation of the Hops Coordinates in the Basis of a Four-Hops Link[a]

	Distance from the transmitter	Latitude	Longitude
Emitter	0	62.6°S	60.4°W
Hop (1)	1,580	50.4°S	43.6°W
Hop (2)	4,755	23.1°S	27.4°W
Hop (3)	7,930	1.3°N	17.3°W
Hop (4)	11,105	28.2°N	7.1°W
Receiver	12,700	40.8°N	0.5°E

[a]The distance is expressed in kilometers.

is performed in the analog domain. This architecture benefits from the advantages of software radio technology [*Mitola*, 1995], thus overcoming the bandwidth limitation of the previous receivers. The results from this survey are described by *Vilella et al.* [2006c].

[8] In this paper, the final results of the project are presented, corresponding to 60 days of soundings from December 2006 to February 2007. First a brief presentation of the geographical link and sounding equipment is shown in section 2. The sounding technique and algorithms are described in section 3. The results of the survey analysis in terms of link availability, Doppler and multipath spread and SNR are presented in section 4. Finally some concluding remarks are given in section 5.

2. Link and Hardware Description

[9] In this section, some information about the link and a brief description of the sounding hardware are presented. The transmitter is placed in the Spanish Antarctic Base (BAE) Juan Carlos I (62.6°S, 60.4°W), in Livingston Island and the receiver is located in the Observatori de l'Ebre (40.8°N, 0.5°E) in Spain (see Figure 1). As the Spanish Base operates from November to March, the sounder may be run only during the Antarctic summer (approximately from December to February).

[10] The ground path is around 12,700 km. Since the maximum length of a one-hop link is usually considered to be less than 4000 km [*Davies*, 1991], a minimum of four hops are needed to establish this communication. On the basis of this supposition, the approximate coordinates where these hops may take place are shown in Table 1.

[11] The sun's radiation is one of the most relevant parameter that influences the ionospheric propagation of waves. In order to interpret the sounding results, the sunrise and the sunset along the link and through the whole survey must be taken into account. From Figure 2 it can be noted that the maximum inter-day variation of the sunrise and the sunset is observed in the first hop, and is always less than 1 h. Moreover, the sunrise occurs in the four hops with a maximum time difference of around half an hour, while the sunset happens in the first hop around four or five hours later than in the last hop. Since sounding is performed on a 1-h basis, sunrise might be considered simultaneous along the link, while sunset is a gradual phenomenon lasting around four or five hours. We emphasize that both considerations are valid through the survey.

[12] The transmitter and the receiver block diagrams are depicted in Figure 3. A 7.5-m monopole has been used at both sites because of the ease of installation and the acceptable performance it shows in a wide frequency range. The frequency gain flatness is better than 8 dB and the losses are less than 6 dBi in the 5 to 20 MHz band [*Vilella et al.*, 2005a]. The antenna coupler assures a good impedance matching with a measured SWR less than 2 in the frequency range from 5 to 20 MHz. In the Antarctica the monopole was located on the top of a small hill with a clear view to the north–east direction. At the receiver the antenna was installed on a clear grassland sloping down in the direction of the transmitter.

[13] The transmission power amplifier delivers up to 250 watts to the monopole. The output power could not be further increased due to power supply restrictions in the Spanish Antarctic Base. The nonlinearities of the amplifier gain are compensated by the digital platform so that the frequency response flatness is better than 1 dB in the full frequency range. The digital platform is based on a Virtex FPGA from Xilinx and a transmit signal processor and a high speed D/A converter, both from Analog Devices and running at 60 MHz. The transmitter and the receiver are coarse time synchronized by means of GPS.

[14] The receiver has been implemented using a digital direct conversion architecture. In the analog domain only filtering and amplification is performed whereas additional filtering, baseband mixing and sampling frequency decimation are executed in the digital domain. A low noise amplifier (LNA) with a gain of 40 dB is followed by a bank of digitally tunable band pass filters (BPF). The variable gain amplifier (VGA) is programmed once per sounding to adjust the received power level 6 dB below the full scale range of the A/D converter. The A/D is a 14 bits, 60 MHz converter from Analog Devices. In the digital domain, a digital down converter (DDC) mixes the received signal to baseband, filters it and decimates the sampling frequency. The DDC has been implemented using the VHDL language [*Vilella et al.*, 2006b].

3. Measurement Techniques

[15] In this section, the measurement techniques and analysis algorithms are described. The channel is sounded hourly on 25 preselected frequencies. These frequencies have been chosen to span the frequency range of interest, according to interference measurements

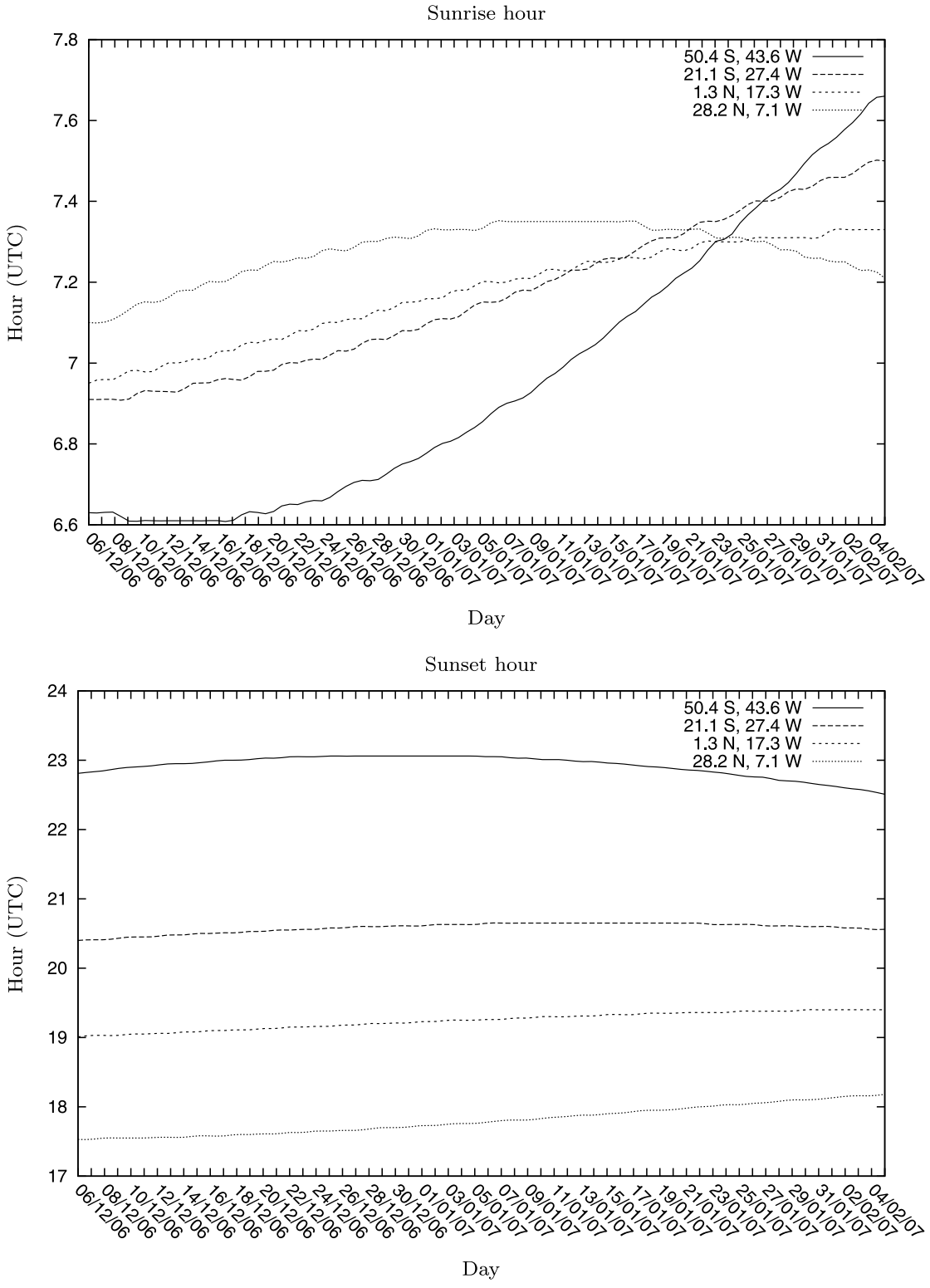

Figure 2. The sunset and the sunrise hours in the four hops indicated in Table 1 through the 2006/2007 survey.

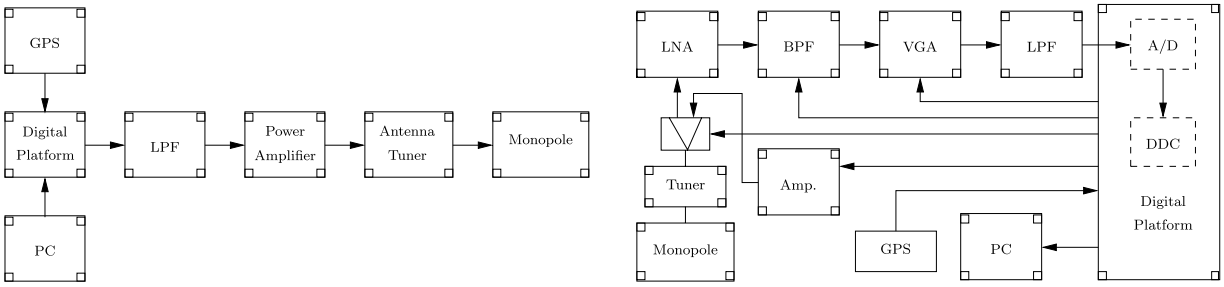

Figure 3. Emitter (left) and receiver (right) block diagrams.

at the receiver site [*Vilella et al.*, 2006a]. Each frequency is sounded as follows:

[16] 1. Approximately 5 s are needed for antenna tuning.

[17] 2. Five seconds are used for narrowband sounding with a full power nonmodulated carrier. This signal is used to measure the communication availability and the frequency drift between the transmitter and the receiver.

[18] 3. Around 15 s are used for a wideband sounding based on a pulse compression technique using pseudo random noise sequences (m-sequences) (*Parsons* [2000]; see Table 2). Then, in the receiver an estimation of the channel impulse response is obtained and time and frequency dispersion parameters are calculated.

[19] Therefore the dwell time at each frequency is around twenty seconds (including narrowband and wideband sounding), and every frequency is revisited every hour.

[20] The block diagram of the algorithms used to estimate the channel impulse response is depicted in Figure 4. Let $r[n]$ be the received signal during the wideband sounding interval. First a frequency synchronization (δf) is applied based on the narrowband sounding detection. Then, the correlation of the received signal with a replica of the emitted pulse-shaped sequence (s_e) is carried out:

$$\phi_{r,s_e}[n] = \sum_{k=0}^{N_e-1} r[n+k]s_e[k] \tag{1}$$

where N_e is the length of s_e. The channel matrix is calculated as:

$$h[n,\tau] = \phi_{r,s_e}[nlN_c + \tau], \quad n \in \left[0, \lfloor \frac{\Delta t F_m}{lN_c} \rfloor - 1\right], \quad \tau \in [0, lN_c - 1] \tag{2}$$

where τ is the delay variable, l is the number of chips of the sounding sequence, N_c is the number of samples per chip, Δt is length of the wideband sounding interval and F_m is the baseband sampling frequency in the receiver. During the 2006/2007 survey, $\Delta t = 15$ s and $F_m = 50$ *kHz*, whereas l and N_c may take different values. An estimation of the scattering function is calculated from the channel matrix [*Proakis*, 1995]:

$$R_s[\tau, \upsilon] = \sum_{\xi} R_h[\xi, \tau] e^{-j2\pi\xi\upsilon} \tag{3}$$

where υ is the Doppler shift variable, ξ is the time variable, and

$$R_h[\xi, \tau] = \sum_{n} h^*[n, \tau] h[n+\xi, \tau] \tag{4}$$

[21] An example of this analysis is depicted in Figure 5, corresponding to the sounding of a frequency around 8 MHz at midnight.

[22] Let $[\tau_1, \tau_2]$ be the multipath observation window and $[\upsilon_1, \upsilon_2]$ the Doppler shift observation window. These

Table 2. Setup Configuration for the Wideband Sounding During the 2006/2007 Survey

			Multipath, ms		Doppler, Hz			
Setup configuration	Sequence length	Chip Rate	Res.	Max.	Res.	Max.	D^{τ} (dB)	D^{υ} (dB)
(1)	63	2500	0.4	25	0.07	20	SNR + 27	SNR + 33
(2)	127	5000	0.2	25	0.07	20	SNR + 30	SNR + 33

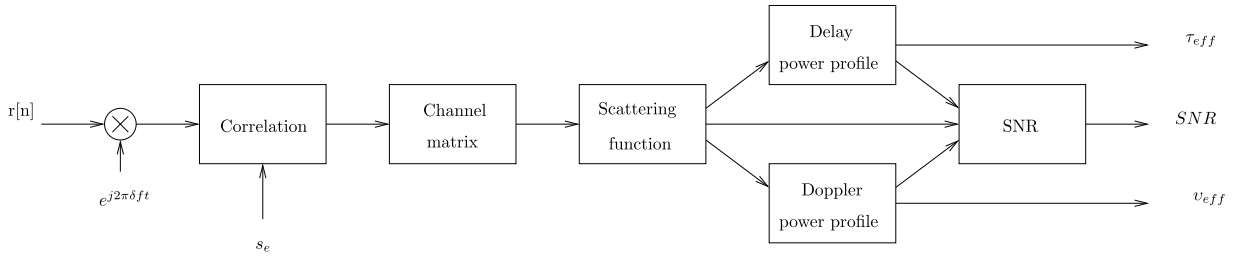

Figure 4. Block diagram of the algorithms applied to estimate the channel impulse response and the corresponding SNR and delay and Doppler spread.

windows have been set according to the maximum measured multipath and Doppler spreads in previous works [*Vilella et al.*, 2005b] to [−3.5, 3.5] (ms) and [−2.5, 2.5] (Hz) respectively. Then, the multipath power profile is calculated as:

$$\phi[\tau] = \sum_{\nu=\nu_1}^{\nu_2} R_S[\tau, \nu] \tag{5}$$

[23] Similarly the Doppler power profile is obtained as:

$$\phi[\nu] = \sum_{\tau=\tau_1}^{\tau_2} R_S[\tau, \nu] \tag{6}$$

[24] The dynamic range of the delay and Doppler power profiles are related to the observation windows. Actually if $r[n]$ is received with a given SNR, then the dynamic range of the multipath power profile measurement with respect to noise (D^{τ}) is determined by:

$$D^{\tau} = SNR + 10\log_{10}\frac{f_c}{\nu_2 - \nu_1} \tag{7}$$

where f_c is the chip frequency. Analogously, the dynamic range of the Doppler power profile measurement with respect to noise ($D\upsilon$) is determined by:

$$D^{\nu} = SNR + 10\log_{10}\frac{\Delta t}{\tau_2 - \tau_1} \tag{8}$$

[25] Next, the spread parameters are calculated. The multipath spread is measured from the multipath power profile as the 80% power spread, with a correction applied for the width of the transmitted pulse and the base noise level. This parameter is called composite multipath spread (τ_{eff}) by *Angling and Davies* [1999]. Analogously the Doppler spread is measured from the Doppler power profile as the 80% power spread, again corrected for the width of the transmitted pulse and the base noise level. This measure is called composite Doppler spread (υ_{eff}) by *Warrington and Stocker* [2003]. Then, the area spread factor is defined as the area enclosed by the composite multipath and Doppler spreads in the scattering function [*Nissen and Bello*, 2003].

[26] Finally an estimation of the SNR may be obtained from the scattering function according to the following equation:

$$SNR = \frac{P|_{Asp} - \rho_n A_{sp}}{\rho_n A} \qquad \rho_n = \frac{P|_{\overline{Asp}}}{\overline{A_{sp}}} \tag{9}$$

where P stands for power, A_{sp} is the area spread factor, A is total area in the scattering function, and $\overline{A_{sp}}$ is the area in the scattering function outside the area spread factor. The term ρ_n is the noise power per unit of area in the scattering function. Note that all uncorrelated signals, including interference signals, contribute to the measured noise level.

[27] The setup configurations for the wideband sounding during the 2006/2007 survey are summarized in Table 2. We note that the sequence length is changed in the same ratio as the chip rate in order to compensate for the variation of the SNR when the sounded bandwidth is modified.

4. Results

[28] In this section, the results from the 2006/2007 survey are presented, corresponding to the soundings performed during 60 days from the 6th December 2006 to the 5th February 2007. The sounder was stopped every day from 13:00 UTC to 18:00 UTC (where the worst propagation conditions exist) for configuration and maintenance purposes. The system employed frequencies ranging from 5 MHz to 17 MHz and the output power was fixed to 200 watts.

[29] In section 4.1 an estimation of the link availability is presented. Next, the multipath and Doppler spread

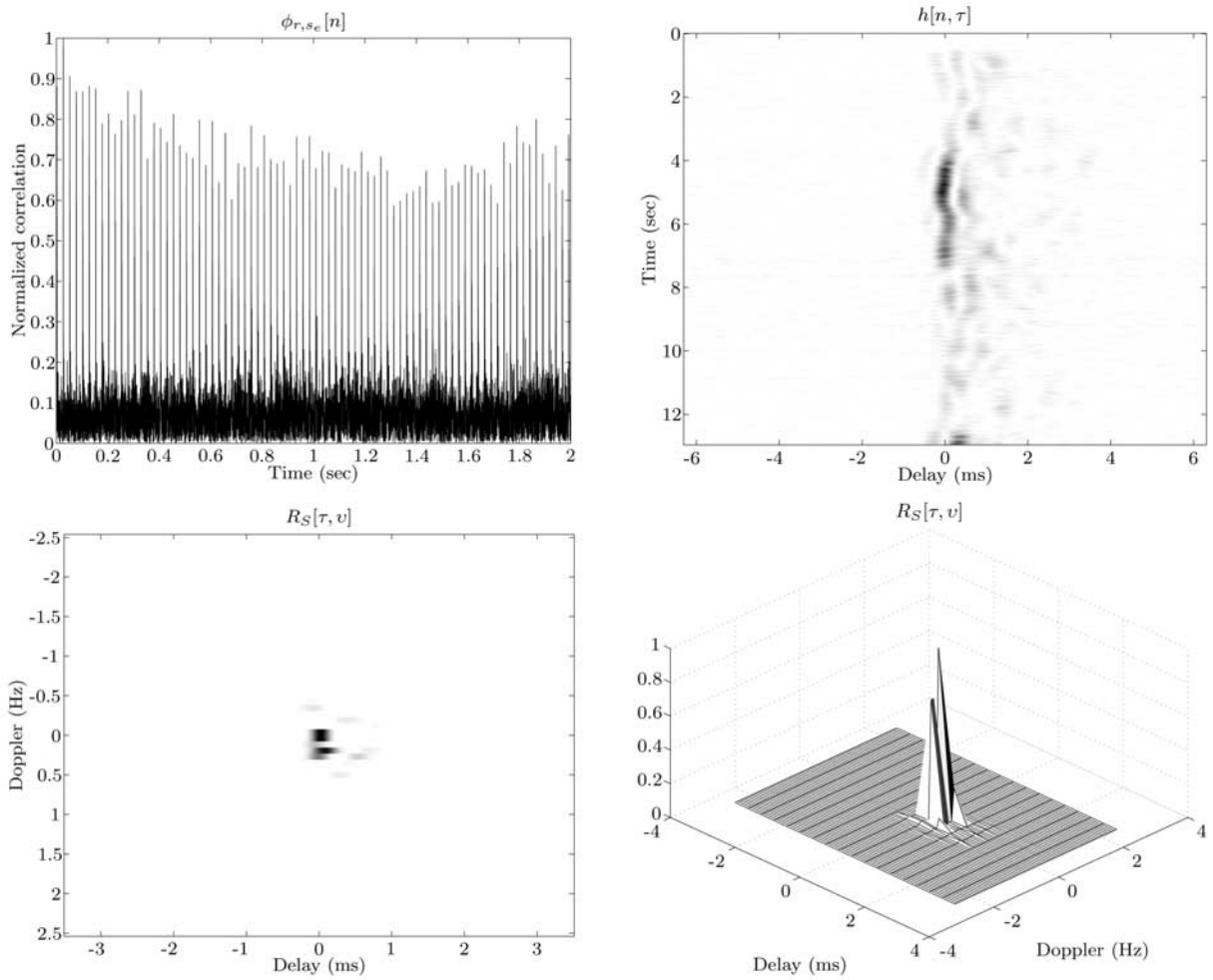

Figure 5. Example of the wideband sounding results. The top left frame corresponds to 2 s of the correlation of the received signal with a replica of the emitted sequence. The channel matrix corresponding to 13 s of analysis is depicted in the top right frame. A two-dimensional and a three-dimensional plot of the normalized scattering function are shown in the bottom frames.

results are shown in section 4.2 and finally an estimation of the median signal-to-noise ratio is presented in section 4.3.

4.1. Link Availability

[30] First, an estimation of the availability of the link is discussed. The availability (and the similar term reliability) is frequently used in the literature referring to the probability for a circuit to achieve a specified performance or a minimum SNR to enable a given quality of service (see, for example, *Goodman et al.* [1997]). In our case, however, the physical layer for data transmission is not yet defined and therefore the required SNR to offer a given service is unknown. In this paper, the term availability is defined as the probability of receiving a tone with a minimum SNR of 6 dB measured in a small bandwidth (10 Hz), as a function of the hour of the day and the frequency of sounding. Since the variation of sunset and sunrise time through the survey is less than one hour an estimation of this measurement may be obtained daily averaging over the whole survey period. This parameter is considered to be strongly related with the ionospheric support for this link.

[31] The estimation of the availability as a function of the hour and the frequency ($d(f,h)$) is depicted in Figure 6. We note the following:

[32] 1. As stated in section 2, the sunset takes place step-by-step along the link, starting around 18 UTC and

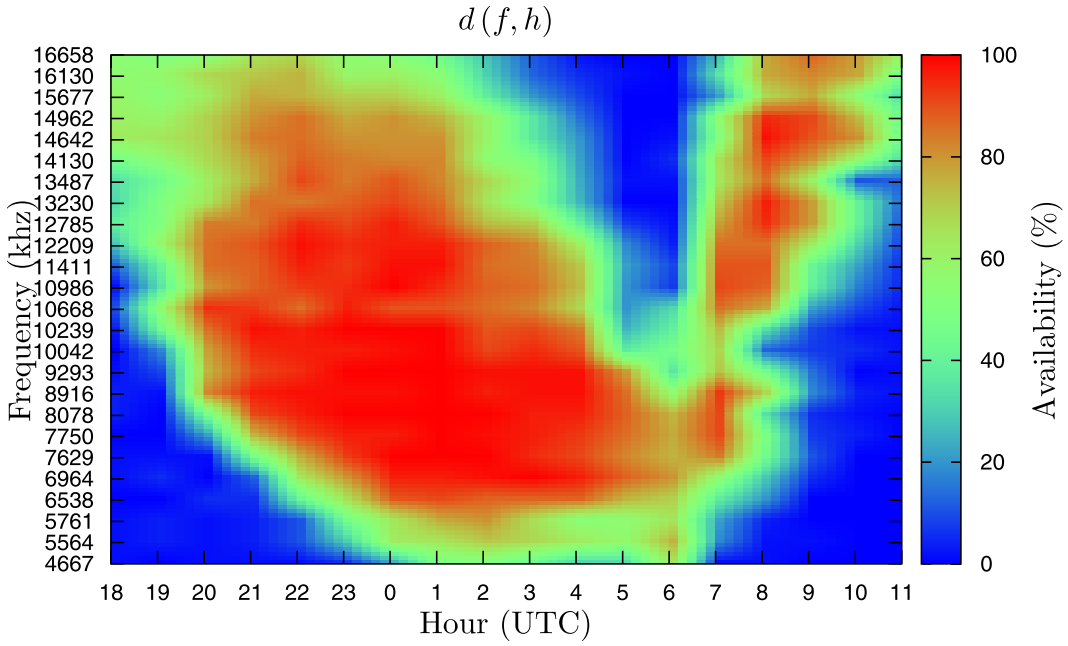

Figure 6. Link availability as a function of the hour of the day and the frequency of sounding.

finishing approximately at 23 UTC. During this interval of time the propagation of frequencies below 12 MHz begins: (1) First, the frequency range between 11 MHz and 12 MHz at 19 UTC; (2) Then, from 9 MHz to 11 MHz at 20 UTC; (3) Finally from 6 MHz to 9 MHz from 20 UTC to midnight. This pattern may be explained by means of these arguments (see Figure 2): (1) The gradual disappearance of the D-layer along the link causes an incremental reduction of the overall attenuation thus permitting lower frequency waves to reach the receiver; (2) The decrease of the electron density in the E- and F-layer increases the virtual height of reflection thus facilitating the establishment of long links.

[33] 2. Between 2 UTC and 5 UTC the propagation of radio waves in the frequency range from 16 MHz to 8 MHz−9 MHz vanishes. This may be due to the decrease of the f_{MUF} along the link.

[34] 3. As stated in section 2 the sunrise occurs within one hour along the link, from 6:30 UTC to 7:30 UTC approximately. From Figure 6 we observe that the propagation of frequencies above 8 MHz−9 MHz suddenly restarts around 7 UTC, coinciding with the sunrise.

[35] 4. From 7 UTC−8 UTC to 11 UTC the availability tends to vanish, beginning with the lower frequency range (5 MHz−6 MHz). This phenomenon may be due to the increase of the attenuation of the D-layer.

[36] We note that our observations are consistent with the frequency support predicted by the ASAPS propagation prediction program [*ASAPS*, 2005].

[37] It is well known that there are strong temporal and frequency variations in HF propagations. Although this information for the link under consideration is clear from Figure 6, a detailed analysis of the link availability as a function of the day, the frequency and the hour may give valuable quantitative information. Next, the daily, hourly and frequency variation of the link availability is investigated.

4.1.1. Daily Variation

[38] The inter-day variation of the availability is measured in terms of the following correlation factor:

$$d(j_n,j_n)^{\rho}=\frac{\sum_{k=1}^{K}\sum_{l=1}^{L} d(f_k,h_l,j_n)d(f_k,h_l,j_m)}{K\cdot L} \qquad (10)$$

where j, f and h denote the day, frequency and hour of sounding, d (f, h, j) is a binary variable that equals one if the tone was successfully received and minus one otherwise, K is the number of frequencies under consideration and L is the number of sounding hours per day. The superscript ρ denotes a correlation measurement. We note that $d(j_n, j_m)^{\rho} \in [-1, 1]$, where one means maximum correlation between days.

[39] The value of $d(j_n, j_m)^{\rho}$ is depicted in Figure 7. A correlation factor of around 0.5 is observed when $j_n \neq j_m$, independently of the value of $|j_n - j_m|$. Therefore the availability between two days differs, in average, in up to 25% of the pairs (f, h). These differences may be mainly

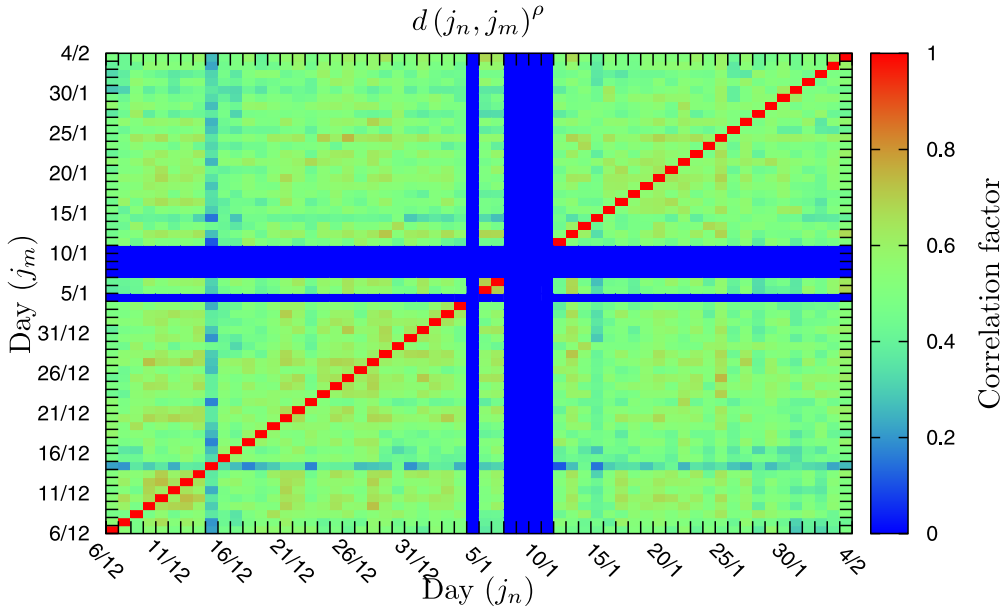

Figure 7. Interday correlation factor according to equation (10). The blue stripes correspond to the days where the sounder was stopped.

due to noise and interference in the receiver site and variability in the ionosphere.

4.1.2. Hourly Variation

[40] The hourly variation of the availability is calculated as:

$$d(h_n, h_m)^\rho = \frac{\sum_{k=1}^{K}\sum_{l=1}^{L} d(f_k, h_m, j_l)\, d(f_k, h_n, j_l)}{K \cdot L} \qquad (11)$$

where K is the number of sounded frequencies and L is the number of days of the survey. This correlation factor measures the stationarity of the ionosphere in terms of its availability, through the day and computing all the frequencies as a whole. The result of this analysis is depicted in Figure 8 (left frame), together with a plot of the pairs (h_n, h_m) with $d(h_n, h_m)^\rho \geq 0.5$ (right frame). We note that (1) an abrupt variation is observed between 6 UTC and 7 UTC, coinciding with the sunrise along the link; (2) the larger stationarity takes place between 23 UTC and 4 UTC; (3) it is worth pointing out the similarity between 18 UTC–19 UTC and 9 UTC–10 UTC, as well as between 23 UTC and 7 UTC. Thus a symmetry between the sunset and the sunrise is observed.

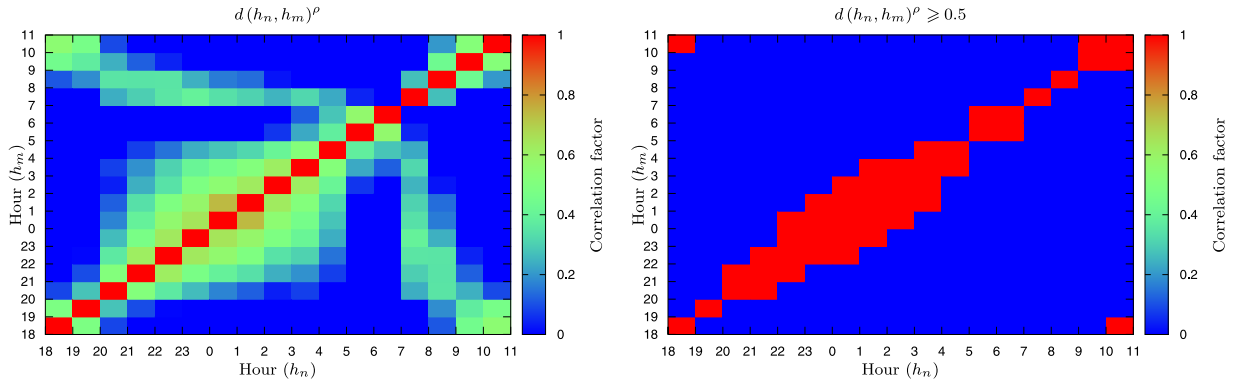

Figure 8. Hourly variation $d(h_n, h_m)^\rho$ as defined in equation (11) (left) and a plot of the pairs (h_n, h_m) with $d(h_n, h_m)^\rho \geq 0.5$ (right).

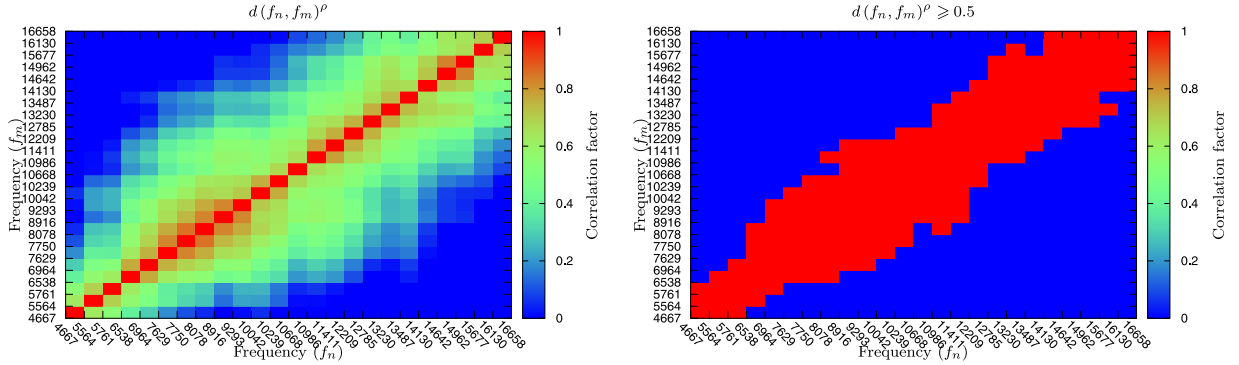

Figure 9. Frequency variation of the availability as defined in equation (12) (left) and a plot of the pairs (f_n, f_m) with d(f_n, f_m)$^\rho \geq 0.5$ (right).

4.1.3. Frequency Variation

[41] In like manner as in the previous sections, the frequency variation of the availability is evaluated as follows:

$$d(f_n,f_m)^\rho = \frac{\sum_{k=1}^{K}\sum_{l=1}^{L} d(f_n,h_k,j_l)d(f_m,h_k,j_l)}{K \cdot L} \qquad (12)$$

where K is the number of sounding hours per day and L is the number of days per survey.

[42] This correlation factor and the plot of the pairs (f_n,f_m) with $d\,(f_n,f_m)^\rho \geq 0.5$ are depicted in Figure 9. Except for the lowest frequencies, a bandwidth of around 4 MHz with a correlation factor of $d\,(f_n,f_m)^\rho \geq 0.5$ is observed.

4.2. Multipath and Doppler Spread Measurements

[43] When considering the design of a communications system both the multipath and Doppler spreads are of major importance. Next, the results of the measurement of that dispersion parameters according to the algorithms described in section 3 are presented. We note that from the setup configurations depicted in Table 2 it follows that the dynamic range of the Doppler and multipath measures is, at least, 27 dB bigger than the received SNR. Thus even for slightly negative SNR in the receiver the reliability of the dispersion measurements is guaranteed (the SNR measures are discussed later in section 4.3).

[44] First, the mean composite multipath spread is shown in Figures 10 and 11. Every figure corresponds to a different hour or group of hours. Many consecutive hours have been grouped in a single figure when the resulting 95% mean confidence interval is improved. The zero values in the figures indicate null data. These considerations will also apply to the mean composite Doppler spread results to be discussed later.

[45] We note the following:

[46] 1. In general, the multipath spread decreases as the frequency increases, with values ranging approximately from 2.25 ms to 0.6 ms. This may be due to the major prevalence of multimoded propagation at lower frequencies.

[47] 2. The maximum multipath spread ranging from 2 ms to 2.5 ms occurs: (1) Between 0 UTC and 4 UTC around 7 MHz; (2) In the time interval from 22 UTC to 3 UTC between 8 MHz and 9 MHz; (3) In the frequency range from 9 MHz to 11 MHz about 23 UTC.

[48] 3. The minimum dispersion values are observed at higher frequencies: around 0.75 ms of multipath spread between 21 UTC and 0 UTC and about 0.5 ms between 9 UTC and 11 UTC at 16658 kHz.

[49] With regard to the mean composite Doppler spread, the results of the analysis are shown in Figures 12 and 13. We observe the following:

[50] 1. With few exceptions, the composite Doppler spread ranges from 1 Hz to 1.5 Hz from the sunset to 4 UTC−5 UTC.

[51] 2. The maximum Doppler spread is around 1.5 Hz and has been measured under different conditions, such as at 9293 kHz about midnight and at 10668 kHz between 22 UTC and 0 UTC.

[52] 3. The minimum Doppler spread is about 0.5 Hz and was observed at the higher frequencies at sunrise, e.g. between 8 UTC and 11 UTC at 16130 kHz.

[53] 4. At some frequencies (e.g. between 8 MHz and 10 MHz and at 11 MHz) a slightly decreasing tendency of the composite Doppler spread is observed from 21 UTC−22 UTC to 4 UTC−5 UTC, varying between 1.5 ms and 1 ms. At other frequencies (e.g. 10 MHz, 12 MHZ, 13 MHz, 15 MHz) the frequency dispersion is approximately constant in that time interval.

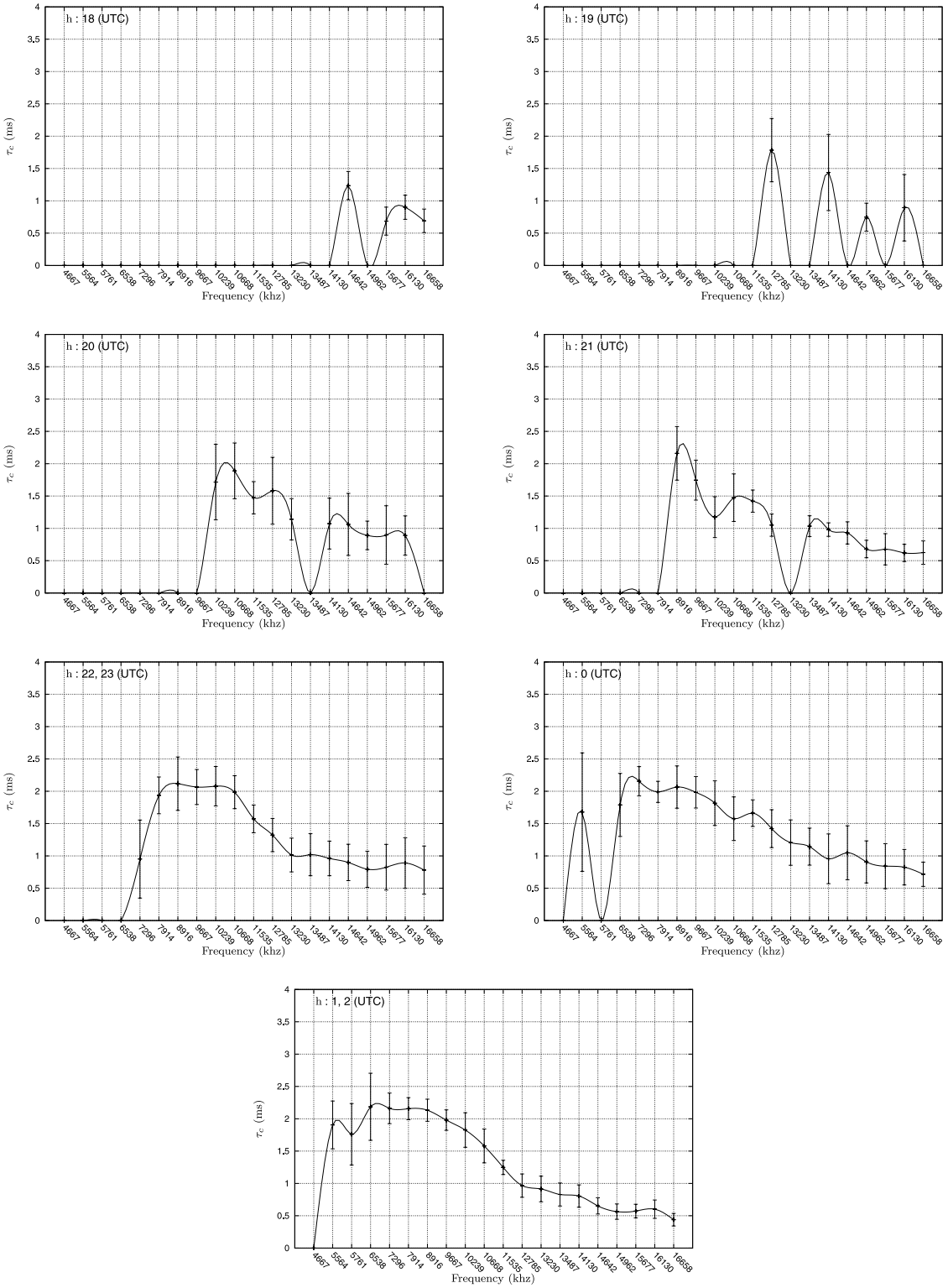

Figure 10. The composite multipath spread as a function of the frequency, measured at different hours (from 18 UTC to 2 UTC). The errors bars denote the 95% mean confidence interval.

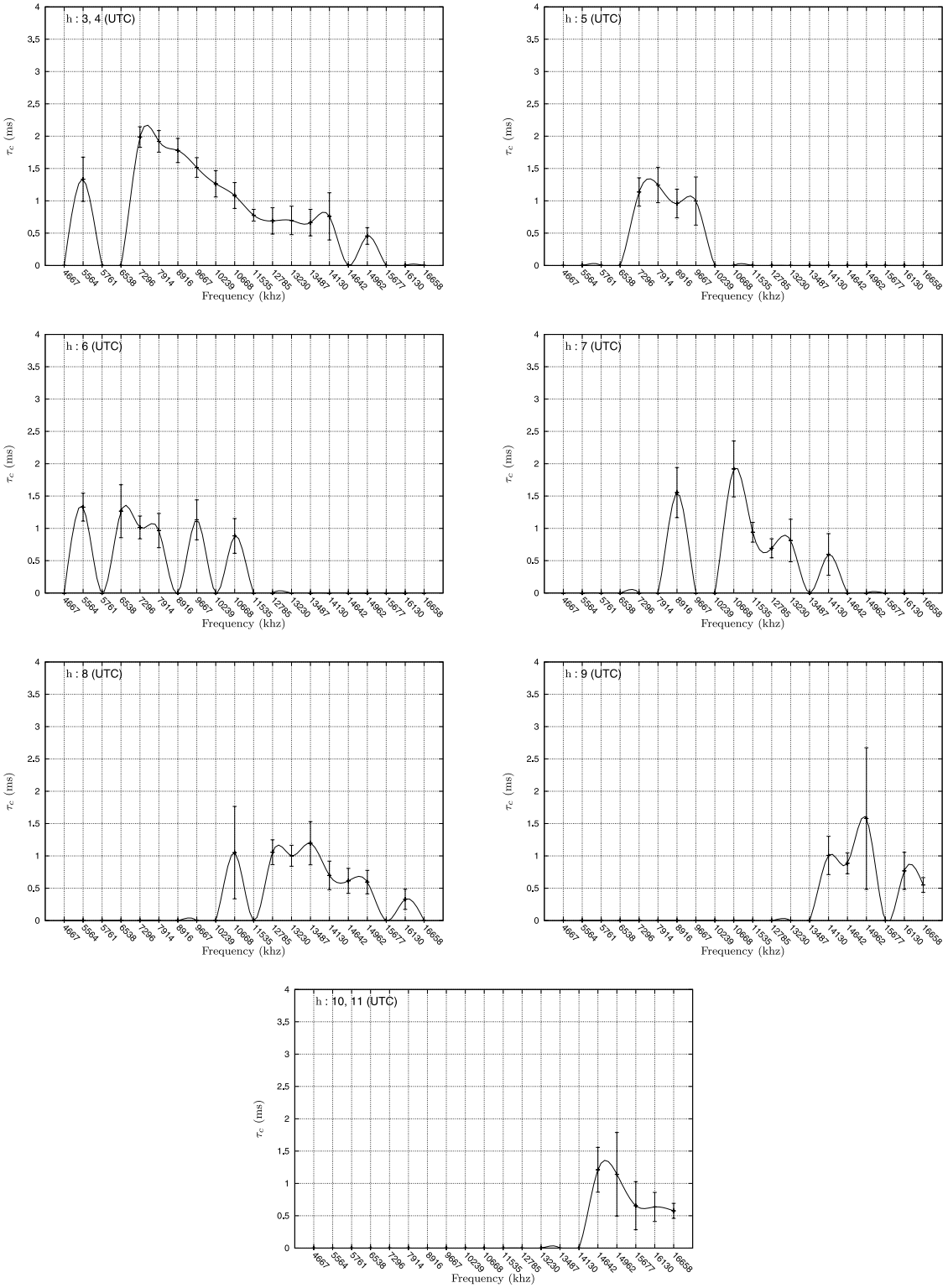

Figure 11. The composite multipath spread as a function of the frequency measured at different hours (from 3 UTC to 11 UTC). The errors bars denote the 95% mean confidence interval.

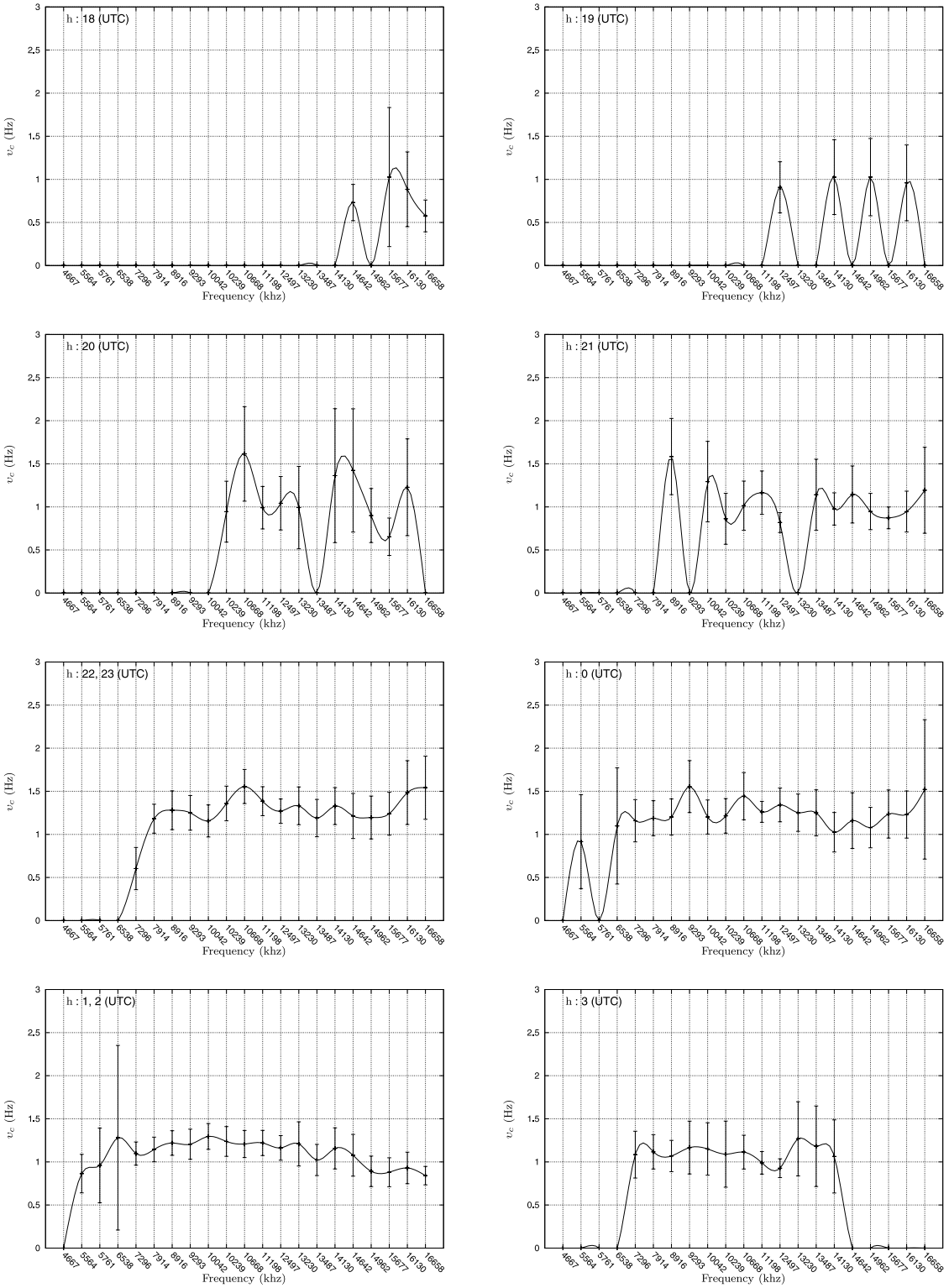

Figure 12. The composite Doppler spread as a function of the frequency measured at different hours (from 18 UTC to 3 UTC). The errors bars denote the 95% mean confidence interval.

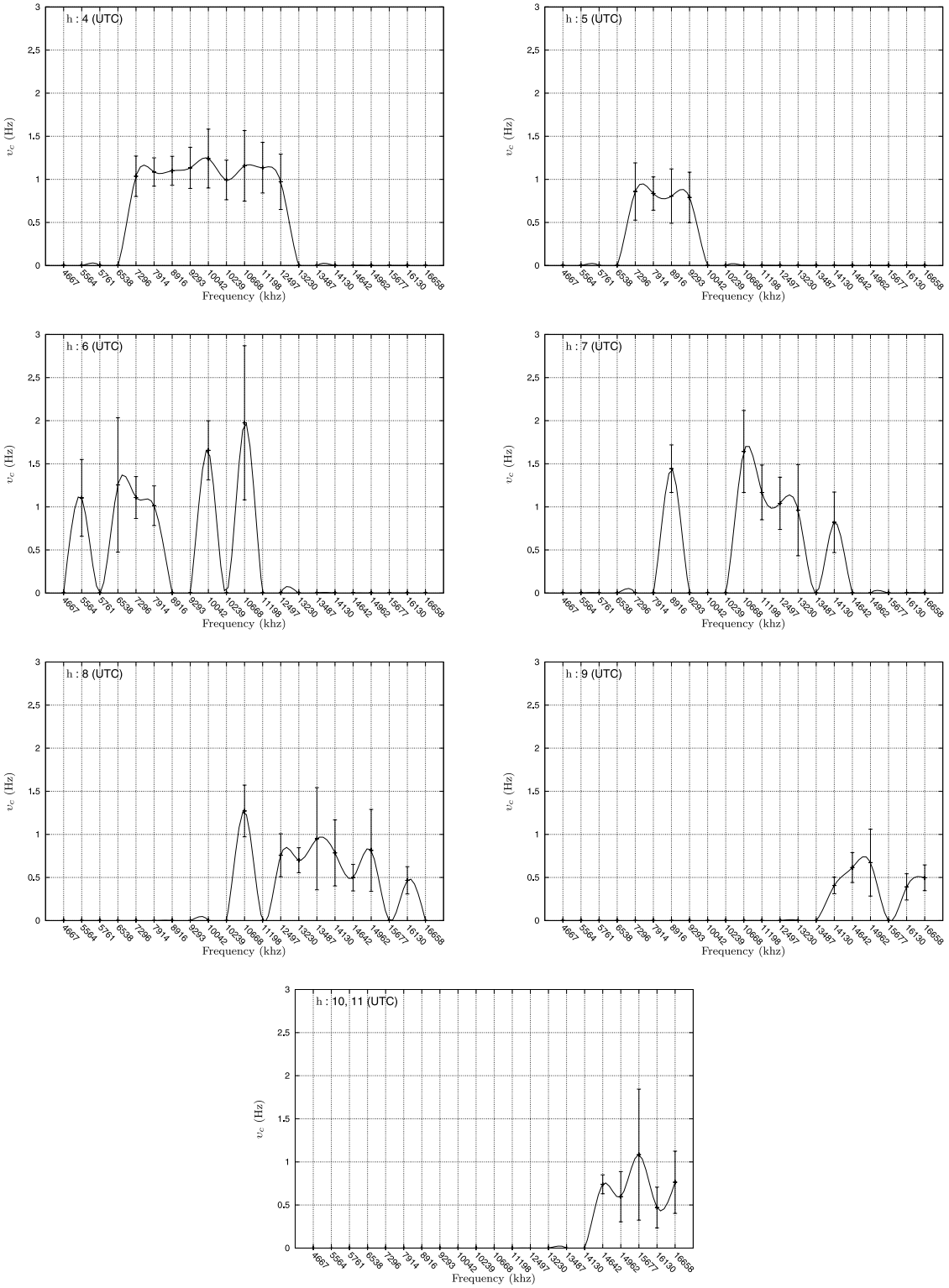

Figure 13. The composite Doppler spread as a function of the frequency measured at different hours (from 4 UTC to 11 UTC). The errors bars denote the 95% mean confidence interval.

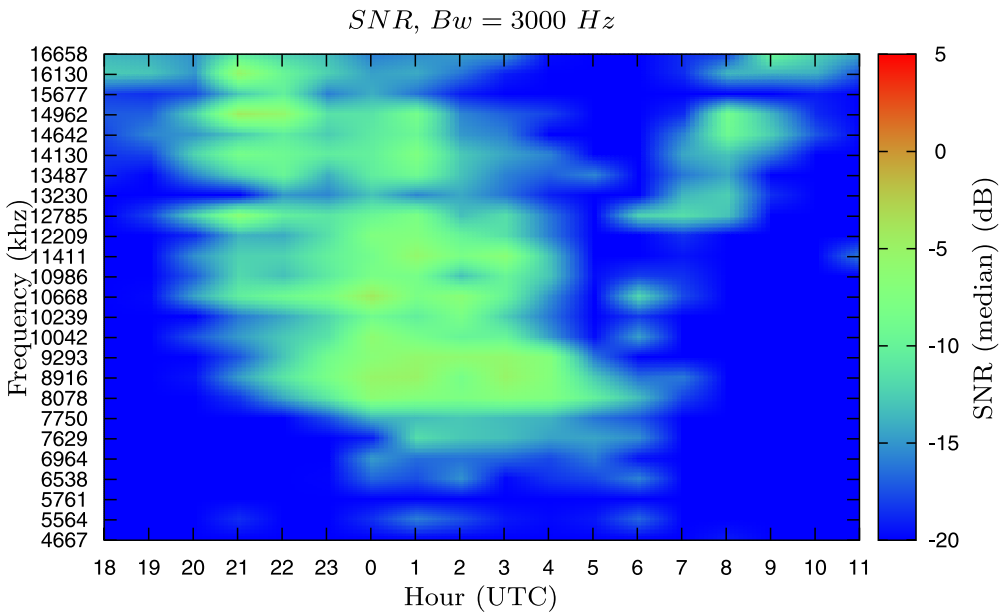

Figure 14. SNR (median) as a function of the frequency and the hour for a 3-kHz bandwidth.

4.3. Median SNR and Maximum Availability

[54] In this section, the measurement of the SNR as a function of the frequency and the time is presented. The plot is expressed in terms of the median so that every result may be interpreted in terms of the SNR exceeded in 50% of the cases. We notice that the SNR measurement is highly dependent on the equipment employed in the channel probe, e.g. transmit power and antenna characteristics. Therefore this result and the corresponding comments should be treated with caution.

[55] The measurement results of the SNR is depicted in Figure 14, where a 3 kHz bandwidth is considered. We notice the large area between 8 MHz and 13 MHz, and 0 UTC and 4 UTC with a SNR ranging from −8 dB to −4 dB. Those levels are also sporadically observed above 13 MHz between 21 UTC and 1 UTC. When different bandwidths are considered, a variation of the noise power approximately proportional to the variation

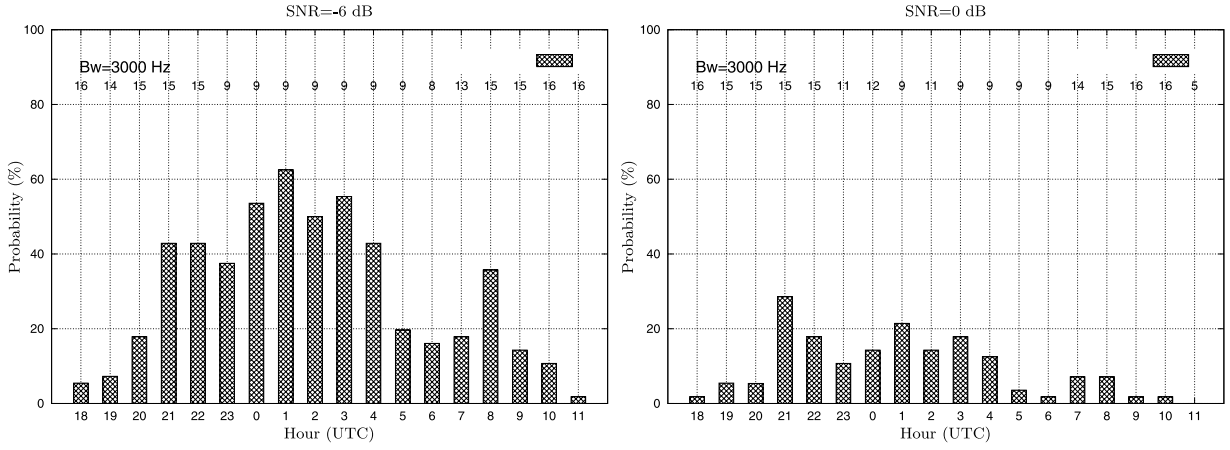

Figure 15. A plot of the frequencies with the maximum probability to exceed a given SNR at every hour measured in a 3-kHz bandwidth.

Table 3. List of the Frequencies With the Maximum Probability to Exceed a −6 dB SNR Threshold at Every Hour Measured in a 3-kHz Bandwidth[a]

Hour	P (SNR > −6 dB), %	Frequency	τ_{eff}	υ_{eff}
20	18	15	0.9	0.7
21	43	15	0.7	0.9
22	43	15	0.8	1.25
23	38	9	2.1	1.2
00	54	9	2.1	1.5
01	63	9	2	1.25
02	50	9	2	1.25
03	55	9	1.6	1.2
04	42	9	1.6	1.2
05	20	9	1	0.8
06	16	8	1	1
07	18	13	0.8	0.95
08	36	15	0.6	0.8
09	14	15	1.5	0.7

[a]The table includes the corresponding probability and the composite multipath and Doppler spreads.

of the signal bandwidth is measured (e.g. around −5 dB and 2 dB for 1 kHz and 5 kHz respectively).

[56] Although some interpretation of these results might be made in terms of ionosphere, it is likely that the antenna radiation characteristics influence these measurements.

[57] On the basis of Figure 14, the frequency with the maximum probability to exceed a given SNR at every hour can be obtained. Figure 15 shows the best frequencies to be used at every hour for two different SNR thresholds: −6 dB and 0 dB in a 3 kHz bandwidth. The analysis is based on the SNR measurements, and therefore its conclusions should be taken with caution. However, its results are of main interest when considering the establishment of a link based on that equipment.

[58] The general tendency shows that when the −6 dB SNR threshold is considered, the best availability is achieved from midnight to 4 UTC (approximately) around 9 MHz, while at 0 dB the optimum is obtained around 21 UTC at higher bands (15 MHz). This may be interpreted in terms of interference: the dense spectral occupancy at low and mid bands impedes obtaining a relatively high SNR, that is, when the SNR threshold increases the availability at low and mid bands rapidly decreases. On the other hand, at higher bands the influence of the interference is lower and the decrease of availability for high SNR threshold is smoother.

5. Concluding Remarks

[59] In this paper, the results from a 60-day sounding survey of an Antarctica to Spain ionospheric link have been presented. The measurements include availability, multipath and Doppler spread and SNR.

[60] It is important to highlight the strong correlation that exists between the sunset and sunrise hour intervals along the link and the frequency availability for that link. In this context, we notice that in terms of signal-to-noise ratio, the frequency range between 8 MHz and 10 MHz is the best alternative between 23 UTC and 6 UTC, while the frequencies above 13 MHz exhibit a better availability before 23 UTC and after 6 UTC.

[61] With regard to multipath and Doppler spread, two time intervals are observed: (1) From 23 UTC to 4 UTC–5 UTC, coinciding with the absence of solar radiation along the link, the composite multipath spread decreases when the frequency increases whereas the composite Doppler spread is approximately flat in frequency. This period of time exhibits typical spread values of 1.5 ms and 1 Hz; (2) From 18 UTC to 23 UTC and from 5 UTC–6 UTC to 11 UTC the multipath and Doppler spread are strongly variable. This is partially due to the changes that take place in the ionosphere during the sunrise and sunset.

[62] A summary of these measures is depicted in Table 3, where the frequencies with the maximum probability to exceed a −6 dB SNR threshold at every hour have been selected and the corresponding composite multipath and Doppler spread are included.

[63] These results are the starting point for the design of a physical layer for data transmission from remote sensors in the Antarctica. This physical layer will be based on a direct sequence spread spectrum technique using turbo coding and adaptive spreading and modulation to match the channel conditions.

[64] **Acknowledgments.** This work has been funded by the Spanish government under the projects REN2003-08376-C02-01, CGL2005-24213-E, and CGL2006-12437-C02-01.

[65] C. Vilella would like to thank J. R. Regué for his advice. We would also like to thank the reviewers for their detailed and useful comments.

References

Angling, M. J., and N. C. Davies (1999), An assessment of a new ionospheric channel model driven by measurements of multipath and Doppler spread, in *IEE Colloquium on Frequency Selection and Management Techniques for HF Communications*, pp. 4/1–4/6, 29–30 March.

Angling, M. J., P. S. Cannon, N. C. Davies, T. J. Willink, V. Jodalen, and B. Lundborg (1998), Measurements of Doppler and multipath spread on oblique high latitude HF paths and their use in characterizing data modem performance, *Radio Sci.*, *33*(1), 97–107.

ASAPS, Australian IPS Radio and Space Services (2005), ASAPS for Windows version 5.2, Sydney, NSW, Australia. (Available at www.ips.gov.au).

Davies, K. (1991), *Ionospheric Radio*, Peter Peregrinus Ltd., London.

Fitzgerald, T. J., P. E. Argo, and R. C. Carlos (1999), Equatorial spread F effects on an HF path: Doppler spread, spatial coherence, and frequency coherence, *Radio Sci.*, *34*(1), 167–178.

Gibson, A. J., U. M. Yilmaz, Y. Tulunay, C. B. Erol, A. Özgü, and T. Ata (1995), Characteristics of fading of HF signal and noise intensities of three paths between the United Kingdom and Turkey, *Radio Sci.*, *30*(3), 649–658.

Goodman, J., J. Ballard, and E. Sharp (1997), A long-term investigation of the HF communication channel over middle- and high-latitudes paths, *Radio Sci.*, *32*(4), 1705–1715.

Mitola, J. (1995), The software radio architecture, *IEEE Commun. Mag.*, *33*(5), 26–38.

Nissen, C. A., and P. A. Bello (2003), Measured channel parameters for the disturbed wide-bandwidth HF channel, *Radio Sci.*, *38*(2), 1023, doi:10.1029/2002RS002746.

Parsons, J. D. (2000), *Mobile Radio Propagation Channel*, John Wiley and Sons, New York.

Proakis, J. G. (1995), *Digital Communications*, McGraw-Hill, New York.

Rao, S. V. B., T. R. Rao, V. G. Reddy, D. R. Lakshmi, B. Veenadhari, R. S. Dabas, I. Ahmed, and M. M. Gupta (2002), HF radio signal fading and atmospheric radio noise measurements at low latitudes, *Radio Sci.*, *37*(5), 1083, doi:10.1029/2001RS002495.

Vilella, C., D. Miralles, J. C. Socoró, J. L. Pijoan, and R. Aquilué (2005a), A new sounding system for HF digital communications from Antarctica, in *Proc. International Symposium on Antennas and Propagation*, Seoul, 3–5 August.

Vilella, C., J. C. Socoró, D. Miralles, J. L. Pijoan, and P. Bergadà (2005b), HF channel measurements for digital communications from Antarctica, in *Proc. International Ionospheric Effects Symposium*, Washington, 3–5 May.

Vilella, C., D. Badia, J. L. Pijoan, M. Deumal, M. Ribó, and J. R. Regué (2006a), On site receiver testing. Application to long distance HF links, in *Proc. International Symposium on Electromagnetic Compatibility EMC Europe 2006*, Barcelona, 4–6 September.

Vilella, C., P. Bergadà, M. Deumal, J. L. Pijoan, and R. Aquilué (2006b), Transceiver architecture and Digital Down Converter design for long distance, low power HF ionospheric links, in *Proc. Ionospheric Radio Systems and Techniques*, pp. 95–99, London, 18–21 July, doi:10.1049/cp:20060311.

Vilella, C., J. C. Socoró, J. L. Pijoan, I. Gutiérrez, and D. Altadill (2006c), An Antarctica to Spain HF Link. Oblique Sounding Results, in *Proc. Ionospheric Radio Systems and Techniques*, pp. 91–94, London, 18–21 July, doi:10.1049/cp:20060310.

Wagner, L. S., J. A. Goldstein, M. A. Rupar, and E. J. Kennedy (1995), Delay, Doppler, and amplitude characteristics of HF signals received over a 1300-km transauroral sky wave channel, *Radio Sci.*, *30*(3), 659–676.

Warrington, E. M., and A. J. Stocker (2003), Measurements of the Doppler and multipath spread of the HF signals received over a path oriented along the midlatitude trough, *Radio Sci.*, *38*(5), 1080, doi:10.1029/2002RS002815.

D. Miralles, J. L. Pijoan, and C. Vilella, Grup de Recerca en Electromagnetisme i Comunicacions (GRECO), Enginyeria i Arquitectura La Salle, Universitat Ramon Llull, Quatre Camins, 2, 08022 Barcelona, Spain. (carlesv@salle.url.edu)